Journal of Power Sources 237 (2013) 98–103

Contents lists available at SciVerse ScienceDirect

Journal of Power Sources

journal homepage: www.elsevier.com/locate/jpowsour

Thermodynamic studies on Sn–Na alloy in an intermediate temperature ionic liquid NaFSA–KFSA at 363 K

Takayuki Yamamoto [a], Toshiyuki Nohira [a,*], Rika Hagiwara [a,*], Atsushi Fukunaga [a,b], Shoichiro Sakai [b], Koji Nitta [b], Shinji Inazawa [b]

[a] Graduate School of Energy Science, Kyoto University, Yoshida-honmachi, Sakyo-ku, Kyoto 606-8501, Japan
[b] Sumitomo Electric Industries Ltd., 1-1-3 Shimaya, Konohana-ku, Osaka 554-0024, Japan

HIGHLIGHTS

- Thermodynamic studies were conducted on Sn–Na alloys in NaFSA–KFSA at 363 K.
- Galvanostatic intermittent titration technique was employed.
- A potential–Na composition curve was obtained during alloy formation.
- $Na_{15}Sn_4$ and α-NaSn phases were detected by *ex situ* X-ray diffraction analysis.
- The formation potentials of several Sn–Na alloys were determined.

ARTICLE INFO

Article history:
Received 16 January 2013
Received in revised form
21 February 2013
Accepted 25 February 2013
Available online 7 March 2013

Keywords:
Sn–Na alloy
Negative electrode
Ionic liquid
Bis(fluorosulfonyl)amide
Equilibrium potential
Galvanostatic intermittent titration technique

ABSTRACT

The equilibrium potentials for Sn–Na alloy formation reactions are investigated in an intermediate temperature ionic liquid, NaFSA–KFSA ($x_{NaFSA} = 0.56$, $x_{KFSA} = 0.44$, FSA = bis(fluorosulfonyl)amides), at 363 K. Galvanostatic intermittent titration technique (GITT) is employed to obtain the potential–Na composition curve of the Sn–Na alloy. *Ex situ* X-ray diffraction (XRD) analysis reveals that plateaus at 0.16 and 0.08 V vs. Na^+/Na in the potential–Na composition curve correspond to α-NaSn/Na_9Sn_4 and $Na_9Sn_4/Na_{15}Sn_4$ two-phase states, respectively. Although distinct potential plateaus are not observed, the equilibrium potentials of β-Sn/$NaSn_2$ and $NaSn_2$/α-NaSn are suggested to be 0.53 and 0.46 V vs. Na^+/Na, respectively. Finally, the Gibbs free energies of formation of the Sn–Na alloys are calculated and compared with reported data.

1. Introduction

Intense efforts have been devoted to the development of sodium secondary batteries, especially in the last decade [1–5]. Previous and current studies on electrolytes in sodium secondary batteries are categorized according to the operating temperature: The first includes those operating at high temperatures of ~573 K, such as Na/S [6,7] and $Na/NiCl_2$ [8,9] batteries, while the second includes those operating at ambient temperature. At high temperatures, a solid electrolyte such as β"-alumina ($Na_2O{\cdot}xAl_2O_3$, $5 \leq x \leq 7$) is adopted, while liquid electrolytes such as organic solvents and aqueous solutions [1–4], are employed for ambient temperature operation. Batteries operating at ambient temperature have many advantages owing to their lower operating temperature, including easier handling, no need for heaters, and a variety of available component materials. However, there are safety issues when the batteries are scaled up because of the flammability and volatility of the organic solvents. Aqueous solutions are also not ideal for batteries with high energy densities owing to their narrower electrochemical windows. Therefore, the development of new electrolytes with improved safety and performance is required.

Accordingly, we developed a new class of ionic liquid that has a wide electrochemical window and is capable of reversible

* Corresponding authors. Tel.: +81 75 753 5822; fax: +81 75 753 5906.
E-mail addresses: nohira@energy.kyoto-u.ac.jp (T. Nohira), hagiwara@energy.kyoto-u.jp (R. Hagiwara).

0378-7753/$ – see front matter © 2013 Elsevier B.V. All rights reserved.
http://dx.doi.org/10.1016/j.jpowsour.2013.02.076

electrodeposition of metallic sodium [10–14]. We previously reported the physicochemical and electrochemical properties of NaFSA–KFSA eutectic melts (x_{NaFSA} = 0.56, x_{KFSA} = 0.44, m.p. = 334 K; FSA = bis(fluorosulfonyl)amide) [13]. This intermediate temperature ionic liquid (ITIL) is unique since it consists entirely of inorganic ions. The eutectic melt exhibits a reasonably high ionic conductivity of 3.3 mS cm^{-1} and a wide electrochemical window of approximately 5.2 V, as well as the capacity for sodium metal deposition/dissolution at 363 K [15]. Our previous study also demonstrated that a $NaCrO_2$ positive electrode exhibited good cyclability over 100 cycles in this ITIL at 353 K [15]. Thus, a sodium secondary battery containing this ITIL is expected to have high performance and safety. However, when sodium metal is used as the negative electrode, its dendritic deposition may cause a safety issue. In addition, the operating temperature of a battery that uses sodium metal is limited to below the melting point of sodium (371 K). Therefore, it is necessary to develop a new negative electrode material that is safer and has a wider operation temperature range.

Tin is known to form eight intermetallic compounds with sodium at 363 K [16] and is therefore attractive as a negative electrode for sodium secondary batteries. According to the phase diagram of the Sn–Na system [16] (Fig. 1), the most Na-rich compound is $Na_{15}Sn_4$, which has a high theoretical capacity of 847 mA h $(g\text{-}Sn)^{-1}$. Since Sn–Na alloys have considerably higher melting points (>493 K) than sodium metal, the problem of the temperature limits for battery operation is solved. There are several reports concerning Sn–Na alloy negative electrodes. Chevrier and Ceder predicted formation potentials for some Sn–Na alloys using density functional theory (DFT) calculations [17]. Slater et al. reported that several potential plateaus were observed, suggesting the coexistence of Sn–Na alloys in an electrolyte containing an organic solvent at ambient temperature [2]. Komaba et al. investigated the cyclability of Sn powder electrodes with a polyacrylate binder [18]; they obtained a high reversible capacity of 500 mA h $(g\text{-}Sn)^{-1}$ in an FEC-added $NaClO_4$/PC electrolyte at ambient temperature and confirmed the formation of a $Na_{15}Sn_4$ phase by *ex situ* XRD analysis. Ellis et al. observed a structural change during the alloying/dealloying of tin with sodium in an $NaPF_6$/EC-DEC electrolyte at ambient temperature using *in situ* XRD analysis [19]. However, most of the obtained XRD patterns did not agree with any of the reported Sn–Na phases. In our previous study [20], the charge–discharge behavior of a Sn-film negative electrode was investigated in NaFSA–KFSA ionic liquid at 363 K. As shown in Fig. 2, at a current density of 0.619 mA cm^{-2} with cut-off voltages of 0.005 and 1.200 V, three potential plateaus were observed in both the charging (a, b, and c) and discharging (a′, b′, and c′)processes, respectively. Considering the observed capacity at each potential plateau and the theoretical values for each Sn–Na alloy, the three discharge plateaus were tentatively assigned as follows: (a′) α-NaSn/Sn (observed capacity: ~200 mA h $(g\text{-}Sn)^{-1}$,theoretical capacity: 226 mA h $(g\text{-}Sn)^{-1}$); (b′) Na_9Sn_4/α-NaSn (observed capacity: ~250 mA h $(g\text{-}Sn)^{-1}$,theoretical capacity: 282 mA h $(g\text{-}Sn)^{-1}$); and (c′) $Na_{15}Sn_4/Na_9Sn_4$ (observed capacity: ~300 mA h $(g\text{-}Sn)^{-1}$,theoretical capacity: 339 mA h $(g\text{-}Sn)^{-1}$). However, the Sn–Na alloy phases were not directly confirmed.

From this background, in the present study, we investigated the formation potentials of Sn–Na alloy phases at 363 K by galvanostatic intermittent titration technique (GITT) using NaFSA–KFSA ionic liquid and *ex situ* X-ray diffraction (XRD) analysis. To our knowledge, this is the first report that combines GITT and XRD to study Sn–Na alloy formation. There are several papers that report the formation potentials or thermodynamic data of Sn–Na alloys [21–24]; however, most of them focused on liquid alloys [21–23]. Although Crouch-Baker et al. reported the equilibrium potentials of some Sn–Na alloys at 393 K [24], no comprehensive studies on the entire set of Sn–Na alloy phases were conducted. Thus, it is worth investigating the Sn–Na system over the entire compositional range at intermediate temperature. In the final part of the present study, we calculate the Gibbs free energies of the formation of Sn–Na alloys from the corresponding equilibrium potentials at 363 K and compare them with reported data.

2. Experimental

NaFSA (99+%) and KFSA (99+%) were purchased from Mitsubishi Materials Electronic Chemicals Co., Ltd. The salts were dried under vacuum at 353 and 333 K, respectively, for 48 h prior to use. The NaFSA–KFSA eutectic salt (mol% NaFSA:KFSA = 56:44 [13]) was prepared by grinding the two salts in a mortar.

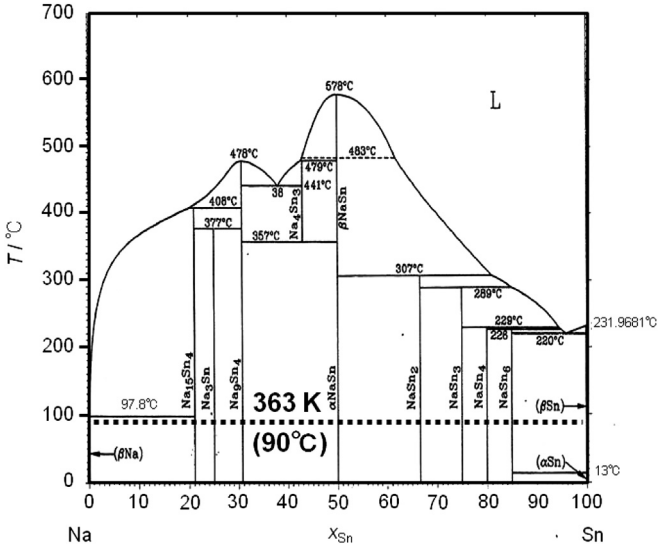

Fig. 1. Binary phase diagram for Sn–Na system [16].

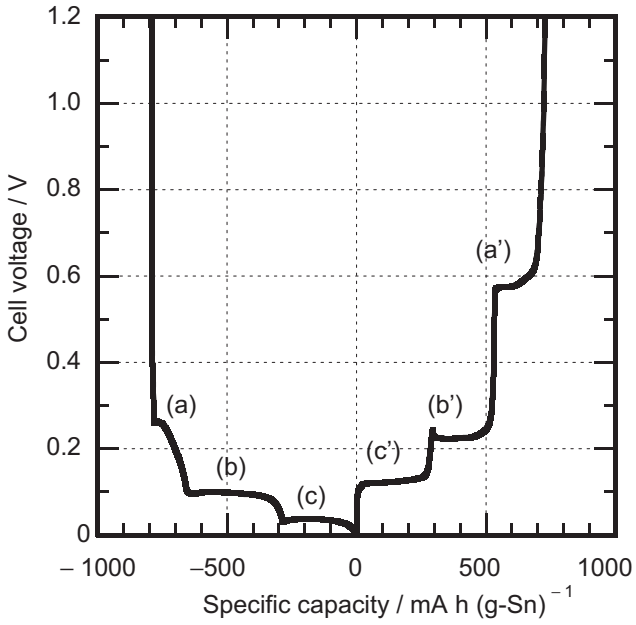

Fig. 2. A charge–discharge curve of the Na/NaFSA–KFSA/Sn cell at 363 K. Cut-off voltages: 0.005 And 1.200 V. Current density: 0.619 mA cm^{-2}. Cycle number: 1. [20].

All electrochemical measurements were performed under argon using a VSP electrochemical measurement apparatus (Bio-Logic Co.) with a two-electrode cell (Tomcell Japan Co., Ltd.). Two sheets of glass-fiber filter paper (Whatman, GF-A, 260 μm) were used as a separator, which was vacuum-impregnated with the electrolyte prior to the test. A Sn film on Al foil was used as the working electrode. The Sn-film electrodes were prepared by electrodeposition of Sn onto Al foil current collectors. The amounts of electrodeposited Sn were determined via inductively coupled plasma atomic emission spectroscopy (ICP-AES). From this data, the thicknesses of the Sn films were calculated to be between 10.9 and 12.0 μm. The counter electrode comprised Na metal (99.85%; Sigma–Aldrich, Inc.). The two-electrode cell was heated using a mantle heater, and the temperature of the cell was monitored using a thermocouple and maintained at 363 K.

Galvanostatic intermittent titration technique (GITT) was employed according to the following procedure:

1. Galvanostatic electrolysis was conducted at a current of C/20 rate for 80 min (*i.e.*, 56.4 mA h $(g\text{-}Sn)^{-1}$, 1/15 of full charge (847 mA h $(g\text{-}Sn)^{-1}$)).
2. The open circuit potential was monitored; when the rate of potential change became less than 1.0 mV h^{-1}, the potential was regarded as the equilibrium value.
3. Steps 1 and 2 were repeated 18 times in total.

The Sn–Na alloy samples were prepared by a combination of galvanostatic and potentiostatic electrolysis. After electrolysis, the open circuit potential was monitored and the potential just before cooling the cell was regarded as the potential of each Sn–Na alloy sample. After removal of the NaFSA–KFSA salts using dehydrated and deoxidized tetrahydrofuran (water content < 10 ppm, oxygen content < 1 ppm; Wako Pure Chemical Industries, Ltd.), the samples were analyzed using an X-ray diffractometer (Ultima IV, Rigaku Co.; Cu-$K\alpha$ radiation ($\lambda = 0.15418$ nm), 40 kV and 40 mA) equipped with a 1D high-speed detector (D/teX Ultra, Rigaku Co.) with a nickel filter. All XRD measurements were conducted in an argon atmosphere using an air-tight cell. Some of the obtained patterns were corrected using a standard specimen of mica and analyzed using the DICVOL program [25].

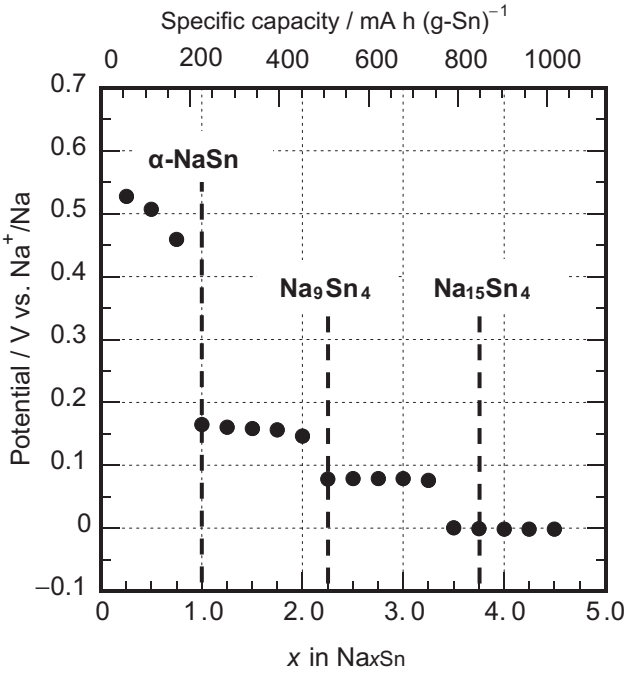

Fig. 3. The relation between equilibrium potential and Na composition for Sn–Na alloy determined by GITT using a Na/NaFSA–KFSA/Sn cell at 363 K.

Table 1
Summary of final Na compositions and potentials for Sn–Na alloy samples.

Sample no.	Final Na composition (x in Na_xSn)	Potential/V vs. Na^+/Na
1	0.03	0.557
2	1.04	0.225
3	2.30	0.122
4	4.14	0.007

3. Results and discussion

3.1. Equilibrium potentials of Sn–Na alloys

According to the phase diagram of the Sn–Na system [16], as shown in Fig. 1, eight intermetallic compounds exist at 363 K: $Na_{15}Sn_4$, Na_3Sn, Na_9Sn_4, α-NaSn, $NaSn_2$, $NaSn_3$, $NaSn_4$, and $NaSn_6$.

Fig. 3 shows the relation between the equilibrium potential and Na composition of the Sn–Na alloys, as determined by GITT in NaFSA–KFSA at 363 K. The Na composition, x, is defined as the atomic ratio of sodium to tin. In the negative potential region below 0.2 V vs. Na^+/Na, three distinct potential plateaus are observed. The capacities of the plateaus at ~0.16 V ($1.0 < x < 2.0$), 0.08 V ($2.25 < x < 3.25$), and 0 V ($3.5 < x < 4.5$) naturally lead to the following estimation: these equilibrium states correspond to Na_9Sn_4/α-NaSn, $Na_{15}Sn_4/Na_9Sn_4$, and $Na_{15}Sn_4$/Na, respectively. The potential reaches 0 V at $x = 3.5$, which is smaller than the theoretical value for the full charge of $x = 3.75$ ($Na_{15}Sn_4$); this is probably due to the slow diffusion of Na in the Sn–Na alloy. A gently sloped region is also observed at ~0.5 V vs. Na^+/Na and $0 < x < 1.0$. According to the phase diagram of the Sn–Na system, several potential plateaus should appear within this Na composition range. However, in the present measurement, the resolution of the Na composition is insufficient to distinguish the plateaus between $0 < x < 1.0$.

On the basis of the results from GITT, Sn–Na alloy samples are prepared by a combination of galvanostatic and potentiostatic electrolysis. Table 1 lists the final Na composition and potential of each Sn–Na alloy sample. The final Na compositions are calculated from the total quantity of electricity assuming 100% current efficiency. The potential values are the open circuit potentials just

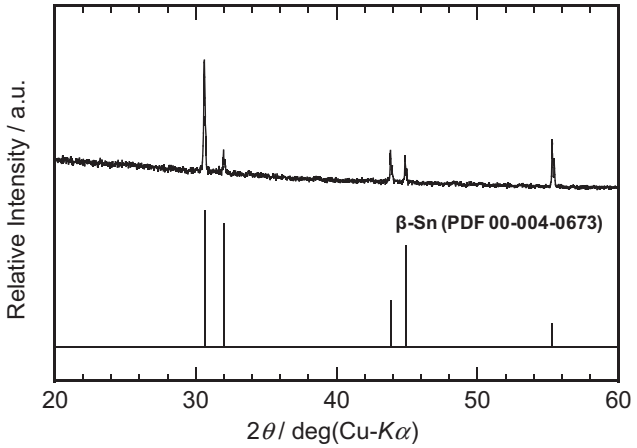

Fig. 4. An XRD pattern of the sample No.1 (potential: 0.557 V vs. Na^+/Na).

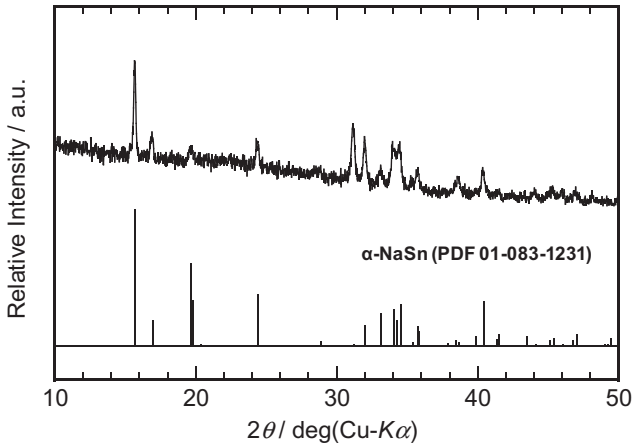

Fig. 5. An XRD pattern of the sample No.2 (potential: 0.225 V vs. Na^+/Na).

before cooling the cell. It should be noted that, for sample 1, Sn is first alloyed to the composition of $Na_{0.24}Sn$ by galvanostatic electrolysis, and then dealloyed by successive potentiostatic electrolysis at 0.600 V, 0.800 V and 1.200 V; the open circuit potential is then monitored and confirmed to be stable at 0.557 V vs. Na^+/Na. The other samples are prepared by only the alloying process.

Fig. 4 shows the XRD pattern of sample 1 (potential: 0.557 V vs. Na^+/Na). The pattern is identified as β-Sn, which confirms that the Sn–Na alloy that formed return to β-Sn. On the assumption of 100% current efficiency, the final Na composition, x (in Na_xSn), of sample 1 is calculated to be 0.03, which is consistent with the XRD result. The XRD pattern of sample 2 (potential: 0.225 V vs. Na^+/Na) is shown in Fig. 5 and shows evidence of α-NaSn, which is consistent with the calculated Na composition of $x = 1.04$. Although the peak for 321 reflection ($2\theta = 31.23°$) is exceptionally intense, this can be explained by the preferred crystal orientation of the sample. Since sample 3 (potential: 0.122 V vs. Na^+/Na) possesses a Na composition of $x = 2.30$, its predicted phase is Na_9Sn_4; however, the obtained XRD pattern shown in Fig. 6 does not match the previously reported pattern for the Na_9Sn_4 phase. It is possible that the electrochemically formed Na_9Sn_4 phase in the present study could have a different structure than the reported one, which is a metallurgically formed Sn–Na alloy. This hypothesis is supported by the fact that the obtained pattern resembles that reported by Ellis et al. [19], who also prepared the Sn–Na alloy using electrochemical methods. However, detailed analysis of the new structure is necessary and

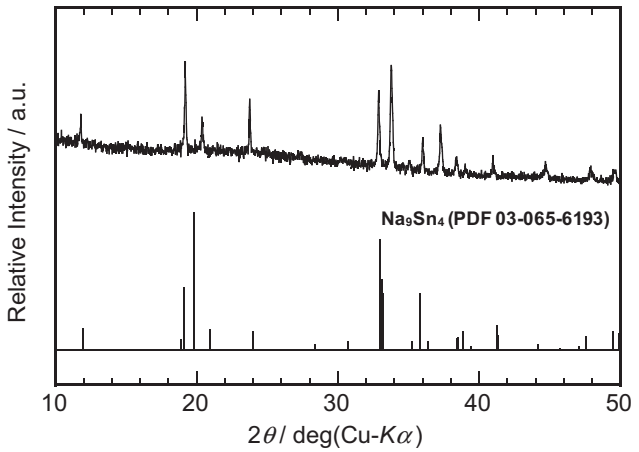

Fig. 6. An XRD pattern of the sample No.3 (potential: 0.122 V vs. Na^+/Na).

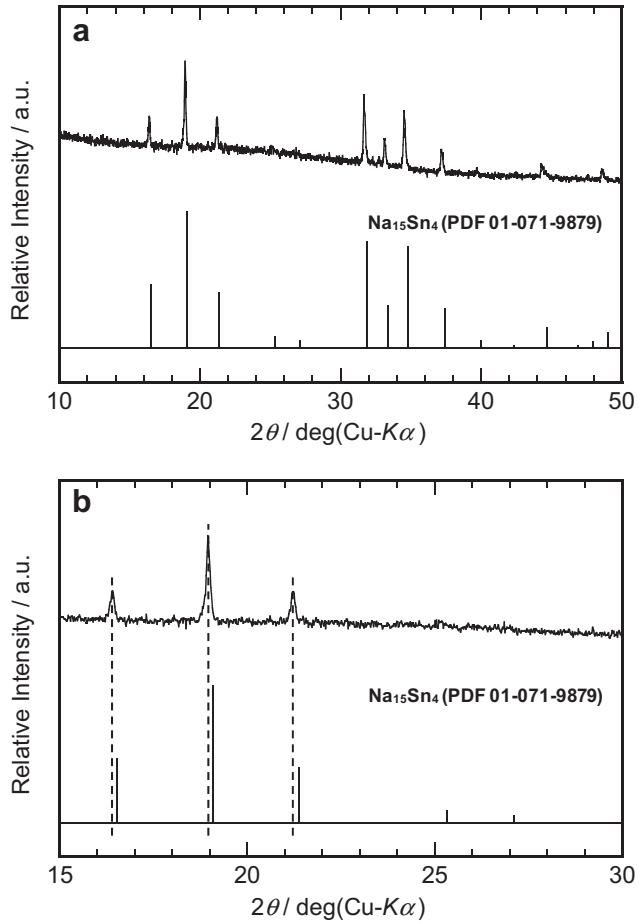

Fig. 7. (a) A full-scale XRD pattern, and (b) a magnified XRD pattern of the sample No.4 (potential: 0.007 V vs. Na^+/Na).

will be performed in the future. The XRD pattern of sample 4 (potential: 0.007 V vs. Na^+/Na) corresponds to the $Na_{15}Sn_4$ phase, as shown in Fig. 7a. However, upon magnification of the profile (Fig. 7b), the peaks are evidently at lower angles than in the reference pattern. Analysis of the XRD pattern using the DICVOL program reveals that the crystal system of this alloy corresponds to a cubic system with a slightly larger lattice parameter ($a = 13.24(1)$ Å) than that of the reference ($a = 13.14$ Å). Table 2 lists the d values and indices of the pattern. The discrepancy in the lattice parameters is likely because of the larger Na composition ($x = 4.14$) than that of the $Na_{15}Sn_4$ phase ($x = 3.75$). Despite $Na_{15}Sn_4$ being considered as a line compound in the phase diagram of Sn–Na system, the results of the present study suggest that it has a compositional range.

By combining the GITT and XRD results, the equilibrium reactions and corresponding potentials for Sn–Na alloys are obtained

Table 2
Observed and calculated d values and indices for sample no.4.

h	k	l	d/Å	
			Obs.	Calc.[a]
2	1	1	5.399	5.407
2	2	0	4.686	4.683
3	1	0	4.180	4.188
3	3	2	2.825	2.824
4	2	2	2.704	2.704
5	1	0	2.598	2.597

[a] $a = 13.24(1)$ Å.

Table 3
Equilibrium reactions and corresponding potentials for Sn–Na alloy in NaFSA–KFSA ($x_{NaFSA} = 0.56$) at 363 K.

Formation reaction	Potential/V vs. Na^+/Na
2 β-Sn + $Na^+ + e^- \leftrightarrows NaSn_2$	0.53
$NaSn_2 + Na^+ + e^- \leftrightarrows$ 2 α-NaSn	0.46
4 α-NaSn + $5Na^+ + 5e^- \leftrightarrows Na_9Sn_4$	0.16
$Na_9Sn_4 + 6Na^+ + 6e^- \leftrightarrows Na_{15}Sn_4$	0.08

and are summarized in Table 3. Although information on the gently sloped region at $0 < x < 1.0$ is not sufficient, a closer look at the more Sn-rich side of the potential–Na composition plots leads to the following assignments: The plots at 0.53 V ($x = 0.25$) and 0.46 V ($x = 0.75$) correspond to coexisting β-Sn/$NaSn_2$ and $NaSn_2$/α-NaSn states, respectively, as indicated by the broken curve in Fig. 8. Concerning this composition region, however, more detailed studies using GITT with closer intervals are necessary, which will be performed in the near future.

3.2. Thermodynamic calculations on the Sn–Na alloy phases

Thermodynamic data for the Sn–Na alloys are obtained as follows: first, relative partial molar Gibbs free energies of Na are obtained from the equilibrium potentials; then, relative partial molar Gibbs free energies of Sn are calculated using the Gibbs-Duhem equation [26]; and finally, standard Gibbs free energies of formation (ΔG_f^0) of −17.0, −23.9, −20.6, and −16.6 kJ (mol-alloy)$^{-1}$ at 363 K are obtained for $NaSn_2$, α-NaSn, Na_9Sn_4, and $Na_{15}Sn_4$, respectively.

These values are compared with previously reported thermodynamic data for Sn–Na alloys. According to Crouch-Baker et al. [24], the equilibrium potentials are 0.44 V (Sn/α-NaSn), 0.16 V (α-NaSn/Na_9Sn_4), and 0.08 V (Na_9Sn_4/$Na_{15}Sn_4$) at 393 K, which corresponds to ΔG_f^0 values of −21.2, −19.0, and −15.4 kJ (mol-alloy)$^{-1}$ for α-NaSn, Na_9Sn_4, and $Na_{15}Sn_4$, respectively. Rivier et al. [21] collected the equilibrium potentials of Sn-rich liquid Sn–Na alloys at different temperatures. Thus, ΔG_f^0 values for liquid Sn–Na alloys can be calculated by Gibbs–Duhem integration using Darken's method [27]. Considering the Sn-rich side of the Sn–Na phase diagram in the range 580–756 K, the activities of Sn and Na of the Sn–Na alloys at the liquidus line are equal to those of α-NaSn. Therefore, it is possible to calculate ΔG_f^0 values for α-NaSn at 580–756 K. Fig. 9 shows the plots of the ΔG_f^0 values for α-NaSn calculated using data from both previous studies and the present study as a function of temperature. The ΔG_f^0 values at 583–633 K calculated using the data of Rivier et al. are plotted at intervals of 10 K, and a solid fitting curve is drawn on the assumption that the ΔH_f^0 and ΔS_f^0 values are independent of temperature except for the fusion of Sn and Na. Thus, the ΔG_f^0 value of α-NaSn is calculated to be −22.4 kJ (mol-alloy)$^{-1}$ at 363 K, which agrees with the value determined in the present study (−23.9 kJ (mol-alloy)$^{-1}$). For reference, the ΔG_f^0 value is reported by Crouch-Baker et al. to be −21.2 kJ (mol-alloy)$^{-1}$ at 393 K [24], which is also close to the calculated value of −22.2 kJ (mol-alloy)$^{-1}$. Thus, the data obtained in the present study is consistent with that reported previously.

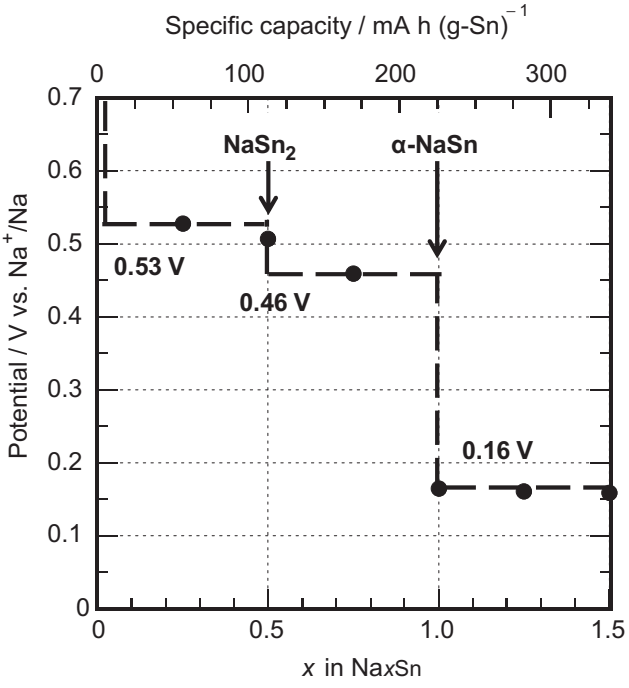

Fig. 8. The relation between equilibrium potential and Na composition for Sn–Na alloy determined by GITT using a Na/NaFSA–KFSA/Sn cell at 363 K (A magnified plot for Sn-rich side of Fig. 3).

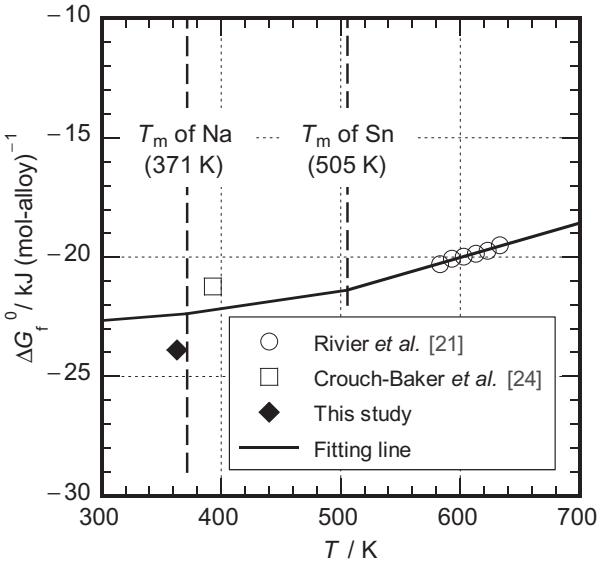

Fig. 9. Comparison of standard Gibbs free energies for formation of α-NaSn calculated from previous studies [21,24] and this study. The solid fitting curve is drawn based on the report by Rivier and Pelton [21] and thermodynamic data of Sn and Na [28].

4. Conclusions

Thermodynamic studies on Sn–Na alloy were conducted in an intermediate temperature ionic liquid, i.e., NaFSA–KFSA, at 363 K. The major findings of the present study are summarized as follows:

1. Using GITT, the equilibrium potential–Na composition plot was obtained. Plateaus at 0.08 and 0.16 V vs. Na^+/Na correspond to the coexisting states of $Na_{15}Sn_4/Na_9Sn_4$ and Na_9Sn_4/α-NaSn, respectively. It is proposed that the gently sloped region at around 0.5 V vs. Na^+/Na is a combination of two plateaus.
2. XRD results were consistent with the equilibrium potential–Na composition plot. The stable phases at 0.557 V, 0.225 V, and 0.007 V vs. Na^+/Na were identified as β-Sn, α-NaSn, and $Na_{15}Sn_4$, respectively. The XRD profile of the alloy at 0.122 V vs. Na^+/Na suggests that the Na_9Sn_4 phase exhibits polymorphism.
3. The equilibrium potentials for several Sn–Na alloys were clarified. Thermodynamic calculations revealed that the ΔG_f^0

value of α-NaSn is −23.9 kJ (mol-alloy)$^{-1}$ at 363 K, which is in agreement with previously reported data.

Acknowledgments

This study was partly supported by the Advanced Low Carbon Technology Research and Development Program (ALCA) of Japan Science and Technology Agency (JST).

References

[1] B.L. Ellis, L.F. Nazar, Curr. Opin. Solid State Mater. Sci. 16 (2012) 168–177.
[2] M.D. Slater, D. Kim, E. Lee, C.S. Johnson, Adv. Funct. Mater. 23 (2013) 947–958.
[3] Y. Kawabe, N. Yabuuchi, M. Kajiyama, N. Fukuhara, T. Inamasu, R. Okuyama, I. Nakai, S. Komaba, Electrochemistry 80 (2012) 80–84.
[4] N. Yabuuchi, H. Yoshida, S. Komaba, Electrochemistry 80 (2012) 716–719.
[5] S.-W. Kim, D.-H. Seo, X. Ma, G. Ceder, K. Kang, Adv. Energy Mater. 2 (2012) 710–721.
[6] J.L. Sudworth, J. Power Sources 11 (1984) 143–154.
[7] T. Oshima, M. Kajita, A. Okuno, Int. J. Appl. Ceram. Technol. 1 (2004) 269–276.
[8] J. Coetzer, J. Power Sources 18 (1986) 377–380.
[9] C.-H. Dustmann, J. Power Sources 127 (2004) 85–92.
[10] R. Hagiwara, K. Tamaki, K. Kubota, T. Goto, T. Nohira, J. Chem. Eng. Data 53 (2008) 355–358.
[11] K. Kubota, K. Tamaki, T. Nohira, T. Goto, R. Hagiwara, Electrochim. Acta 55 (2010) 1113–1119.
[12] K. Kubota, T. Nohira, T. Goto, R. Hagiwara, Electrochem. Commun. 10 (2008) 1886–1888.
[13] K. Kubota, T. Nohira, R. Hagiwara, J. Chem. Eng. Data 55 (2010) 3142–3146.
[14] T. Nohira, T. Ishibashi, R. Hagiwara, J. Power Sources 205 (2012) 506–509.
[15] A. Fukunaga, T. Nohira, Y. Kozawa, R. Hagiwara, S. Sakai, K. Nitta, S. Inazawa, J. Power Sources 209 (2012) 52–56.
[16] T.B. Massalski, Binary Alloy Phase Diagrams, second ed,, ASM International, Ohio, 1990.
[17] V.L. Chevrier, G. Ceder, J. Electrochem. Soc. 158 (2011) A1011–A1014.
[18] S. Komaba, Y. Matsuura, T. Ishikawa, N. Yabuuchi, W. Murata, S. Kuze, Electrochem. Commun. 21 (2012) 65–68.
[19] L.D. Ellis, T.D. Hatchard, M.N. Obrovac, J. Electrochem. Soc. 159 (2012) A1801–A1805.
[20] T. Yamamoto, T. Nohira, R. Hagiwara, A. Fukunaga, S. Sakai, K. Nitta, S. Inazawa, J. Power Sources 217 (2012) 479–484.
[21] M. Rivier, A.D. Pelton, J. Electrochem. Soc. 125 (1978) 1377–1382.
[22] S. Tamaki, T. Ishiguro, S. Takeda, J. Phys. F: Met. Phys. 12 (1982) 1613–1624.
[23] Q. Fang, H. Wendt, J. Appl. Electrochem. 26 (1996) 343–352.
[24] S. Crouch-Baker, G. Deublein, H.-C. Tsai, L.Z. Zhou, R.A. Huggins, Solid State Ionics 42 (1990) 109–115.
[25] A. Boultif, D. Louer, J. Appl. Crystallogr. 37 (2004) 724–731.
[26] O. Kubaschewski, C.B. Alcock, P.J. Spencer, Materials Thermochemistry, sixth ed., Pergamon Press, New York, 1993.
[27] L.S. Darken, J. Am. Chem. Soc. 72 (1950) 2909–2914.
[28] M.J. Bonnie, G. Stanford, R.A. Martin, Thermodynamic Data for Fifty Reference Elements, NASA TP-3287 (1993).